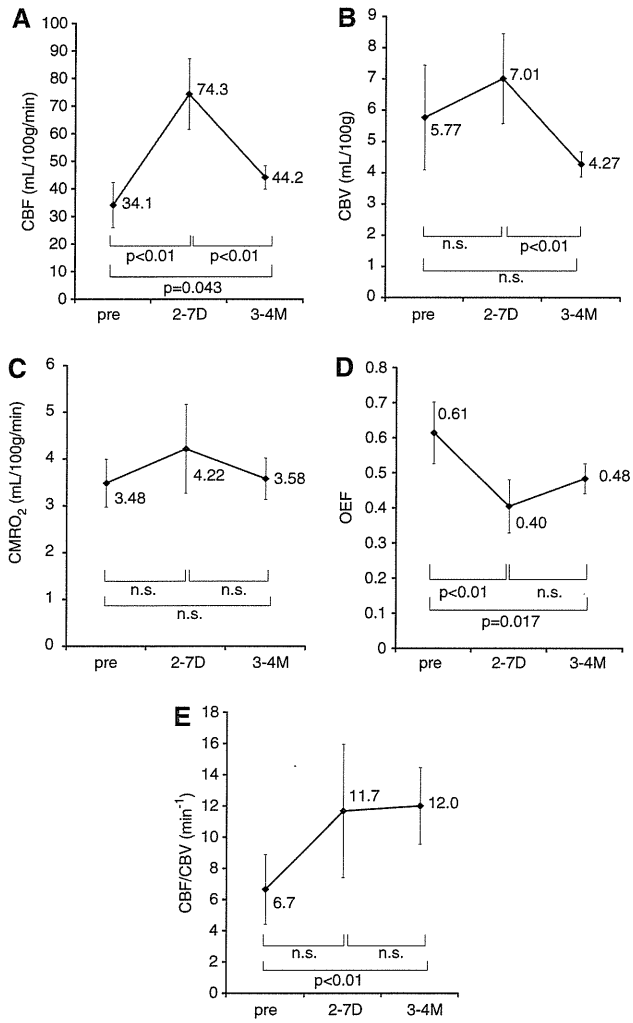

Figure 3 Graphs showing sequential changes in cerebral blood flow (CBF) (**A**), cerebral blood volume (CBV) (**B**), cerebral metabolic rate of oxygen ($CMRO_2$) (**C**), oxygen extraction fraction (OEF) (**D**), and CBF/CBV (**E**) at three different time points: preoperative (pre), subacute postoperative (2 to 7 days (2-7D)), and chronic postoperative (3 to 4 months (3-4M)). Mean values ± standard deviation are shown.

74.3 ± 12.8 mL/100 g per minute ($n = 7$) at the time of hyperperfusion during the subacute stage, and returned to normal levels 3 to 4 months postoperatively (Figure 3A). The preoperative increase in CBV (5.77 ± 1.67 mL/100 g) persisted (7.01 ± 1.44 mL/100 g) during hyperperfusion (normal + 2s.d., 4.12 mL/100 g), and decreased 3 to 4 months postoperatively (Figure 3B). In contrast to interval changes in CBF, $CMRO_2$ increased from 3.48 ± 0.51 to 4.22 ± 0.95 mL/100 g per minute during postoperative hyperperfusion. Interestingly, $CRMO_2$ remained within normal ranges even during hyperperfusion at a peak of 71% (5/7) in the patients. However, the two remaining cases with markedly increased $CMRO_2$ were complicated with postoperative seizures (Figure 3C). As a result, OEF decreased significantly from 0.61 ± 0.09 at baseline to 0.40 ± 0.08 during hyperperfusion (Figure 3D). Cerebral perfusion pressure (CBF/CBV) increased from 6.7 ± 2.2 to 11.7 ± 4.3/min during the subacute stage (Figure 3E). During the follow-up period, values for CBF, $CMRO_2$, and OEF returned to normal levels, while CBV and CBF/CBV showed an improvement over compared with the preoperative values in the region with postoperative hyperperfusion.

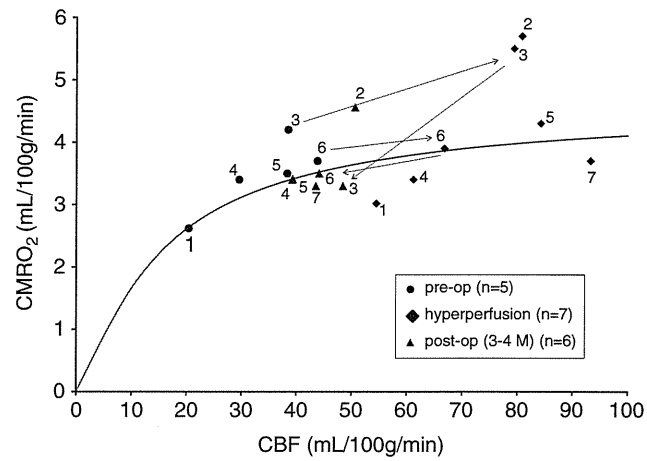

Figure 4 Graph showing the correlation between cerebral blood flow (CBF) and cerebral metabolic rate of oxygen ($CMRO_2$). The Renkin–Crone model (Crone, 1963; Renkin, 1959) was applied to the relationship between CBF and $CMRO_2$. The fitted curve shows that increases in flow lead to smaller changes in $CMRO_2$. The relationship between CBF and $CMRO_2$ almost fits the model for all cases, with the exception of two cases with postoperative seizure, in which the plots were above the curve. Number indicated the case number, respectively.

Comparison of Cerebral Blood Flow with Cerebral Metabolic Rate of Oxygen

Figure 4 shows the correlation between $CMRO_2$ and CBF. The simulated curve shows that increases in CBF lead to smaller changes in $CMRO_2$. Applying the Renkin–Crone model (Crone, 1963; Renkin, 1959) to the relationship between $CMRO_2$ and CBF, the best equation fitting our data for this relationship between them was

$$CMRO_2 = CBF \times OEF = CBF \times (1 - e^{-0.26/CBF}) \quad (1)$$

The fitted curve (Figure 4) showed that the increase in $CMRO_2$ was linear until a flow of ~30 mL/100 g per minute was achieved, and it then increased more gradually as the flow increased. The relationship between CBF and $CMRO_2$ almost fits the Rankin–Crone model (Crone, 1963; Renkin, 1959) with the exception of two cases with postoperative seizure, in which the plots were above the curve.

Representative Case

A 41-year-old woman (case 5) experienced a transient ischemic attack of left-sided sensory disturbance for

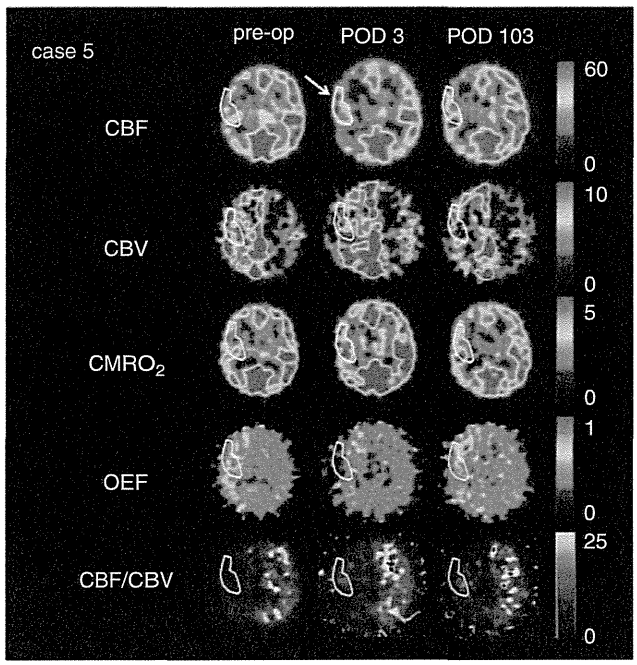

Figure 5 A series of positron emission tomography (PET) studies of a moyamoya disease (MMD) patient (case 5) with symptomatic hyperperfusion. Left: preoperative examinations revealed severe hypoperfusion in the right hemisphere with markedly increased cerebral blood volume (CBV) and oxygen extraction fraction (OEF). CBF/CBV was markedly decreased. Middle: studies obtained on postoperative day 3 showing a marked increase in CBF (white arrow), with persistent increased CBV. Although cerebral metabolic rate of oxygen ($CMRO_2$) was slightly increased, OEF markedly decreased. Right: postoperative examinations obtained 3 months after revascularization. CBF, $CMRO_2$, and OEF were normalized, and CBV and CBF/CBV were improved over the preoperative status. CBF, cerebral blood flow; POD, postoperative day.

a few minutes 5 years ago, and her symptoms gradually worsened. Neuroradiologic examinations showed typical findings compatible with MMD. A PET study indicated misery perfusion on the right hemisphere (Figure 5). The STA-MCA bypass surgery was performed successfully, and she awoke from anesthesia without neurologic deficits. On the third POD, sensory disturbance lasting 30 minutes occurred; similar episodes were repeated several times until the seventh POD. A PET study on POD 3 showed increased CBF and decreased OEF around the anastomotic site. Symptomatic hyperperfusion was diagnosed and her blood pressure was carefully monitored and controlled. Symptoms spontaneously resolved, and the patient was discharged on POD 10.

Discussion

Hyperperfusion Syndrome

Recently, cerebral hyperperfusion has received much attention as a possible cause of transient neurologic dysfunction after bypass surgery for MMD. The main neurologic deficits corresponding to dysfunctions around the bypass site at the perisylvian area include dysarthria, hand motor dysfunction, and motor or sensory dysphasia. Unlike the classical triad of symptoms such as severe unilateral headache, face and eye pain, and seizures and established criteria of CBF after CEA (Piepgras *et al*, 1988; Sundt *et al*, 1981; van Mook *et al*, 2005), a critical definition of CBF using PET, a gold standard, for the diagnosis of hyperperfusion after bypass surgery for MMD remains unestablished.

Here the authors reported, for the first time in MMD, CBF and oxygen metabolism with preoperative and postoperative PET, after screening patients with hyperperfusion first with qualitative ^{123}I-IMP SPECT, the reported definition of postoperative hyperperfusion in MMD, and analyzed the correlation of preoperative PET parameters with development of symptomatic hyperperfusion, and found that preoperative OEF was significantly increase in the patients, whereas no differences were observed in the other parameters. A postoperative PET study, exclusively performed for cases with symptomatic hyperperfusion due to difficult logistic reasons, clearly showed that transient neurologic deterioration due to hyperperfusion was characterized by transient increases in CBF caused by prolonged recovery of CBV, as reported previously in hyperperfusion after CEA and carotid artery stenting (CAS). In terms of oxygen metabolism, however, patients with hyperperfusion were classified into two types, those with normal and elevated $CMRO_2$, respectively, and the latter type was complicated with postoperative seizure.

Diagnosis of Symptomatic Hyperperfusion in Moyamoya Disease

In MMD patients, the incidence of symptomatic hyperperfusion after bypass surgery varies considerably from 21.5% to 38.2% (Fujimura *et al*, 2007, 2011), because of a lack of quantitative evaluation of postoperative CBF and different study populations. Unlike hyperperfusion after CEA, the operational definition of hyperperfusion after bypass surgery for MMD remains unestablished. In this paper, qualitative ^{123}I-IMP SPECT was conducted first during POD 1 to 3 to screen all patients for the presence of hyperperfusion according to the previously reported diagnostic criteria of postoperative hyperperfusion in MMD. The incidence of hyperperfusion on qualitative ^{123}I-IMP SPECT (31%) and symptomatic hyperperfusion (16.7%) in the present study was consistent with the previous report.

Here, the postoperative PET study clearly showed that once symptomatic, mean CBF values increased to 218% of preoperative values, which seems to be consistent with the original concept of post CEA perfusion, and peak CBF values at the subacute postoperative stage were equal to or more than the

control + 2s.d. (57.8 mL/100 g per minute), the predefined value of hyperperfusion on PET calculated from the healthy hemisphere in patients with unilateral stenoocclusive lesions in all cases (Fink *et al*, 1993). This definition based on normal control values seems to be practical since preoperative CBF values on PET may not always be available because of inherent logistic difficulties as in the present study. Taken together, these results indicated that if patients with increased CBF on qualitative ^{123}I-IMP SPECT develop corresponding symptoms postoperatively (the previously reported definition of symptomatic hyperperfusion), peak CBF values measured using PET during subacute stages would be almost consistent with the traditional concept of post CEA hyperperfusion (>100% increase over the baseline) and more than predefined CBF threshold values (control + 2s.d.). The CBF values 3 to 4 months postoperatively remained higher than preoperative values, but returned to normal ranges, indicating that the state of hyperperfusion was temporary.

Mechanism of Hyperperfusion in Moyamoya Disease

Preoperative increases in CBV persisted during hyperperfusion and decreased 3 to 4 months postoperatively, suggesting the prolonged recovery of high CBV values, despite immediate increases in perfusion pressure after direct bypass, may have a key role in the development of hyperperfusion and the associated clinical symptoms lasting for 1 to 14 days in our patients. Accordingly, the preoperative decreased cerebral perfusion pressure increased rapidly within 2 to 7 days of surgery. However, the only PET study on postoperative hyperperfusion after CAS (Matsubara *et al*, 2009) showed significant increases in CBF and CBF/CBV ratios despite the lack of significant changes in CBV during the acute stage. Interestingly, such PET findings were observed in the contralateral hemisphere during the acute stage after CAS. Such differences in temporal changes of PET parameters between MMD and CAS are probably explained by the types of revascularization (high flow or low flow), presence of intracranial arterial stenosis in MMD, and the fact that our study on symptomatic MMD mainly consisted of cases with severe hemodynamic compromise than the CAS PET study (Matsubara *et al*, 2009). Therefore, fundamental mechanisms underlying postoperative hyperperfusion, prolonged recovery of vascular reserve, after bypass surgery for MMD seem to be similar to those after carotid revascularization, although the PET study on carotid stenosis with severe hemodynamic compromise is mandatory to conclude this point. Stringent blood pressure control is similarly necessary for patients with postoperative hyperperfusion in MMD (Fujimura *et al*, 2011), although the blood pressure-lowering effect on the untreated contralateral hemisphere should be carefully considered.

Risk of Symptomatic Hyperperfusion

Decreased vascular reserve on preoperative SPECT images has been reported as a predictor of hyperperfusion syndrome after CEA (Hosoda *et al*, 2001; Ogasawara *et al*, 2003). Cerebral perfusion pressure is generally considered to reflect cerebral vascular reserve and the CBF/CBV ratio is an index of cerebral perfusion pressure (Gibbs *et al*, 1984). Cerebral blood volume is closely related to arteriolar dilatation (Kontos *et al*, 1977; Wahl *et al*, 1970) in response to decreased perfusion pressure distal to hemodynamically significant arterial stenosis. Here, we showed among the preoperative PET parameters that increased OEF was the only significant risk factor for the development of symptomatic hyperperfusion. Also, it is interesting to note that although not significantly different, CBV values tended to be higher in symptomatic hyperperfusion. In this context, Derdeyn *et al* (2002) reported the revised concept of hemodynamic staging using PET and showed that among patients with increased OEF, those with increased CBV may indicate pronounced vasodilatation due to exhausted autoregulatory vasodilatation and be associated with a higher risk of subsequent stroke, whereas those with normal CBV may reflect preserved autoregulatory capacity and be associated with a smaller incidence of subsequent stroke. Taken together, our observations presented in Figure 2B may indicate that even in patients with increased OEF, preoperative increased CBV confers a higher risk of symptomatic hyperperfusion than those with normal CBV. Further studies are necessary to conclude this point.

Cerebral Oxygen Metabolism of Hyperperfusion

The present series consisted of patients with preoperative moderate/severe hemodynamic compromise, and temporary clamping of the recipient arteries may confer additional ischemic insult to the brain adjacent to the anastomotic site during bypass. Previous PET studies in patients with cerebral infarctions showed that rapid perfusion to a cerebrum that has been in a state of chronic ischemia may increase oxygen mechanism (postischemic oxygen hypermetabolism) (Marchal *et al*, 1996, 1999). The postulated mechanisms are (1) overexcitation of cellular metabolism in cells destined to survive or (2) excessive firing of neurons undergoing irreversible damage from a massive release of excitatory amino acids during the period of ischemia or early noxious inflammatory changes. Since no frank infarctions were noted in the area with hyperperfusion on magnetic resonance imaging in subacute or chronic periods in the present study, the above-mentioned overexcitation of cellular metabolism cannot be ruled out as a mechanism underlying postoperative hyperperfusion.

Repetitive neurologic symptoms in patients without overt postoperative convulsion may be caused by

partial seizure. Postoperative seizure is considered to be caused by two basic mechanisms; free radical generation mainly caused by extravascular leakage of blood components, and disturbance of ionic balances across the cell membrane caused by ischemia or hypoxia, both of which are closely linked (Manaka *et al*, 2003). Since postoperative hyperperfusion and seizure share two common underlying mechanisms, that is, free radical generation and ischemic insult, the causal relationship between these two phenomena is difficult to answer conclusively based on this study.

Significant oxygen hypermetabolism was noted only in cases complicated with postoperative seizure. Seizure is an abnormal physiological state that, unlike somatosensory processing, places supranormal demands on autoregulatory mechanisms due to an enormous increase in $CMRO_2$ (Folbergrova *et al*, 1981). During sustained seizures, CBF increases with a corresponding increase in $CMRO_2$ (Brodersen *et al*, 1973; Theodore *et al*, 1996). Our analysis using the Renkin–Crone model (Crone, 1963; Renkin, 1959) showed, with the exception of two cases complicated with seizure, there was no mismatch with CBF and $CMRO_2$. The increased tendency of oxygen hypermetabolism during symptomatic hyperperfusion compared with preoperative or chronic periods even in cases without postoperative seizure was also shown in hyperperfusion after CAS (Matsubara *et al*, 2009). Such oxygen hypermetabolism may explain the sustained neurologic deterioration after bypass surgery for MMD.

Conclusion

This study revealed that symptomatic hyperperfusion in MMD is characterized by temporary increases in CBF >100% over preoperative values caused by prolonged recovery of increased CBV. Among preoperative PET parameters, increased OEF was the only significant risk factor for symptomatic hyperperfusion ($P<0.05$). The causal relationship between seizures and increased $CMRO_2$ during symptomatic hyperperfusion remains unknown.

Disclosure/conflict of interest

The authors declare no conflict of interest.

References

Brodersen P, Paulson OB, Bolwig TG, Rogon ZE, Rafaelsen OJ, Lassen NA (1973) Cerebral hyperemia in electrically induced epileptic seizures. *Arch Neurol* 28:334–8

Crone C (1963) The permeability of capillaries in various organs as determined by use of the 'indicator diffusion' method. *Acta Physiol Scand* 58:292–305

Derdeyn CP, Videen TO, Yundt KD, Fritsch SM, Carpenter DA, Grubb RL, Powers WJ (2002) Variability of cerebral blood volume and oxygen extraction: stages of cerebral haemodynamic impairment revisited. *Brain* 125:595–607

Fink GR, Herholz K, Pietrzyk U, Huber M, Heiss WD (1993) Peri-infarct perfusion in human ischemia: Its relation to tissue metabolism, morphology, and clinical outcome. *J Stroke Cerebrovasc Dis* 3:123–31

Folbergrova J, Ingvar M, Siesjo BK (1981) Metabolic changes in cerebral cortex, hippocampus, and cerebellum during sustained bicuculline-induced seizures. *J Neurochem* 37:1228–38

Fujimura M, Kaneta T, Mugikura S, Shimizu H, Tominaga T (2007) Temporary neurologic deterioration due to cerebral hyperperfusion after superficial temporal artery-middle cerebral artery anastomosis in patients with adult-onset moyamoya disease. *Surg Neurol* 67: 273–82

Fujimura M, Mugikura S, Kaneta T, Shimizu H, Tominaga T (2009) Incidence and risk factors for symptomatic cerebral hyperperfusion after superficial temporal artery-middle cerebral artery anastomosis in patients with moyamoya disease. *Surg Neurol* 71:442–7

Fujimura M, Shimizu H, Inoue T, Mugikura S, Saito A, Tominaga T (2011) Significance of focal cerebral hyperperfusion as a cause of transient neurologic deterioration after extracranial-intracranial bypass for moyamoya disease: comparative study with non-moyamoya patients using N-isopropyl-p-[(123)I]iodoamphetamine single-photon emission computed tomography. *Neurosurgery* 68:957–64; discussion 64–5

Fukui M (1997) Guidelines for the diagnosis and treatment of spontaneous occlusion of the circle of Willis ('moyamoya' disease). Research Committee on Spontaneous Occlusion of the Circle of Willis (Moyamoya Disease) of the Ministry of Health and Welfare, Japan. *Clin Neurol Neurosurg* 99(Suppl 2):S238–40

Furuya K, Kawahara N, Morita A, Momose T, Aoki S, Kirino T (2004) Focal hyperperfusion after superficial temporal artery-middle cerebral artery anastomosis in a patient with moyamoya disease. Case report. *J Neurosurg* 100:128–32

Gibbs JM, Leenders KL, Wise RJ, Jones T (1984) Evaluation of cerebral perfusion reserve in patients with carotid-artery occlusion. *Lancet* 1:182–6

Hosoda K, Kawaguchi T, Shibata Y, Kamei M, Kidoguchi K, Koyama J, Fujita S, Tamaki N (2001) Cerebral vasoreactivity and internal carotid artery flow help to identify patients at risk for hyperperfusion after carotid endarterectomy. *Stroke* 32:1567–73

Iida H, Itoh H, Nakazawa M, Hatazawa J, Nishimura H, Onishi Y, Uemura K (1994) Quantitative mapping of regional cerebral blood flow using iodine-123-IMP and SPECT. *J Nucl Med* 35:2019–30

Iida H, Jones T, Miura S (1993) Modeling approach to eliminate the need to separate arterial plasma in oxygen-15 inhalation positron emission tomography. *J Nucl Med* 34:1333–40

Iida H, Nakagawara J, Hayashida K, Fukushima K, Watabe H, Koshino K, Zeniya T, Eberl S (2010) Multicenter evaluation of a standardized protocol for rest and acetazolamide cerebral blood flow assessment using a quantitative SPECT reconstruction program and split-dose 123I-iodoamphetamine. *J Nucl Med* 51:1624–31

JET Study Group (2002) Japanese EC-IC bypass Trial (JET study): study design and analysis. *Surg Cerebral Stroke* 30:97–100

Kim JE, Oh CW, Kwon OK, Park SQ, Kim SE, Kim YK (2008) Transient hyperperfusion after superficial tem-

poral artery/middle cerebral artery bypass surgery as a possible cause of postoperative transient neurological deterioration. *Cerebrovasc Dis* 25:580–6

Kim KM, Watabe H, Hayashi T, Hayashida K, Katafuchi T, Enomoto N, Ogura T, Shidahara M, Takikawa S, Eberl S, Nakazawa M, Iida H (2006) Quantitative mapping of basal and vasareactive cerebral blood flow using split-dose 123I-iodoamphetamine and single photon emission computed tomography. *Neuroimage* 33:1126–35

Kontos HA, Raper AJ, Patterson JL (1977) Analysis of vasoactivity of local pH, PCO2 and bicarbonate on pial vessels. *Stroke* 8:358–60

Kudomi N, Choi E, Yamamoto S, Watabe H, Kim K, Shidahara M, Ogawa M, Teramoto N, Sakamoto E, Iida H (2003) Development of a GSO detector assembly for a continuous blood sampling system. *IEEE Trans Nucl Sci* 50:70–3

Kudomi N, Hayashi T, Teramoto N, Watabe H, Kawachi N, Ohta Y, Kim KM, Iida H (2005) Rapid quantitative measurement of $CMRO_2$ and CBF by dual administration of ^{15}O-labeled oxygen and water during a single PET scan—a validation study and error analysis in anesthetized monkeys. *J Cereb Blood Flow Metab* 25: 1209–24

Kudomi N, Hayashi T, Watabe H, Teramoto N, Piao R, Ose T, Koshino K, Ohta Y, Iida H (2009) A physiologic model for recirculation water correction in $CMRO_2$ assessment with $^{15}O_2$ inhalation PET. *J Cereb Blood Flow Metab* 29:355–64

Kuroda S, Houkin K (2008) Moyamoya disease: current concepts and future perspectives. *Lancet Neurol* 7:1056–66

Manaka S, Ishijima B, Mayanagi Y (2003) Postoperative seizures: epidemiology, pathology, and prophylaxis. *Neurol Med Chir* 43:589–600

Marchal G, Furlan M, Beaudouin V, Rioux P, Hauttement JL, Serrati C, de la Sayette V, Le Doze F, Viader F, Derlon JM, Baron JC (1996) Early spontaneous hyperperfusion after stroke. A marker of favourable tissue outcome? *Brain* 119(Part 2):409–19

Marchal G, Young AR, Baron JC (1999) Early postischemic hyperperfusion: pathophysiologic insights from positron emission tomography. *J Cereb Blood Flow Metab* 19:467–82

Matsubara S, Moroi J, Suzuki A, Sasaki M, Nagata K, Kanno I, Miura S (2009) Analysis of cerebral perfusion and metabolism assessed with positron emission tomography before and after carotid artery stenting. *J Neurosurg* 111:28–36

Nezu T, Yokota C, Uehara T, Yamauchi M, Fukushima K, Toyoda K, Matsumoto M, Iida H, Minematsu K (2012) Preserved acetazolamide reactivity in lacunar patients with severe white-matter lesions: ^{15}O labeled gas and H_2O positron emission tomography studies. *J Cereb Blood Flow Metab* 32:844–50

Ogasawara K, Komoribayashi N, Kobayashi M, Fukuda T, Inoue T, Yamadate K, Ogawa A (2005) Neural damage caused by cerebral hyperperfusion after arterial bypass surgery in a patient with moyamoya disease: case report. *Neurosurgery* 56:E1380

Ogasawara K, Yukawa H, Kobayashi M, Mikami C, Konno H, Terasaki K, Inoue T, Ogawa A (2003) Prediction and monitoring of cerebral hyperperfusion after carotid endarterectomy by using single-photon emission computerized tomography scanning. *J Neurosurg* 99: 504–10

Piepgras DG, Morgan MK, Sundt TM, Jr, Yanagihara T, Mussman LM (1988) Intracerebral hemorrhage after carotid endarterectomy. *J Neurosurg* 68:532–6

Powers WJ (1991) Cerebral hemodynamics in ischemic cerebrovascular disease. *Ann Neurol* 29:231–40

Renkin EM (1959) Transport of potassium-42 from blood to tissue in isolated mammalian skeletal muscles. *Am J Physiol* 197:1205–10

Sundt TM, Jr, Sharbrough FW, Piepgras DG, Kearns TP, Messick JM, Jr, O'Fallon WM (1981) Correlation of cerebral blood flow and electroencephalographic changes during carotid endarterectomy: with results of surgery and hemodynamics of cerebral ischemia. *Mayo Clin Proc* 56:533–43

Suzuki J, Takaku A (1969) Cerebrovascular 'moyamoya' disease. Disease showing abnormal net-like vessels in base of brain. *Arch Neurol* 20:288–99

Takahashi JC, Miyamoto S (2010) Moyamoya disease: recent progress and outlook. *Neurol Med Chir (Tokyo)* 50: 824–32

Theodore WH, Balish M, Leiderman D, Bromfield E, Sato S, Herscovitch P (1996) Effect of seizures on cerebral blood flow measured with ^{15}O-H_2O and positron emission tomography. *Epilepsia* 37:796–802

van Mook WN, Rennenberg RJ, Schurink GW, van Oostenbrugge RJ, Mess WH, Hofman PA, de Leeuw PW (2005) Cerebral hyperperfusion syndrome. *Lancet Neurol* 4:877–88

Wahl M, Deetjen P, Thurau K, Ingvar DH, Lassen NA (1970) Micropuncture evaluation of the importance of perivascular pH for the arteriolar diameter on the brain surface. *Pflugers Arch* 316:152–63

Journal of Cerebral Blood Flow & Metabolism (2012) 32, 1757–1764

www.jcbfm.com

Reproducibility of cerebral blood flow assessment using a quantitative SPECT reconstruction program and split-dose ^{123}I-iodoamphetamine in institutions with different γ-cameras and collimators

Hiroshi Yoneda[1], Satoshi Shirao[1], Hiroyasu Koizumi[1], Fumiaki Oka[1], Hideyuki Ishihara[1], Kunitsugu Ichiro[2], Tetsuhiro Kitahara[3], Hidehiro Iida[4] and Michiyasu Suzuki[1]

[1]*Department of Neurosurgery and Clinical Neuroscience, Yamaguchi University School of Medicine, Yamaguchi, Japan;* [2]*Department of Public Health, Yamaguchi University School of Medicine, Yamaguchi, Japan;* [3]*Department of Neurosurgery, Ogori Daiichi General Hospital, Yamaguchi, Japan;* [4]*Department of Biomedical Imaging Advanced Medical Engineering Division, National Cerebral and Cardiovascular Center-Research Institute, Osaka, Japan*

Single photon emission computed tomography (SPECT) is used widely in clinical studies. However, the technique requires image reconstruction and the methods for correcting scattered radiation and absorption are not standardized among SPECT procedures. Therefore, quantitation of cerebral blood flow (CBF) may not be constant across SPECT models. The quantitative SPECT (QSPECT) software package has been developed for standardization of CBF. Using the QSPECT/dual-table autoradiographic (DTARG) method, CBF and cerebral vascular reactivity (CVR) at rest and after acetazolamide challenge can be evaluated using ^{123}I-iodoamphetamine in a single SPECT session. In this study, we examined the reproducibility of quantitative regional CBF and CVR in QSPECT/DTARG using different SPECT models at two facilities. The subjects were nine patients with chronic cerebral ischemic disease who underwent QSPECT/DTARG at both facilities with use of different γ-cameras and collimators. There were significant correlations for CBF at rest and after acetazolamide challenge measured at the two facilities. The consistency of the CBFs of the patients measured at the two facilities were good in all cases. Our results show that CBF measured by QSPECT/DTARG in the same patients is reproducible in different SPECT models. This indicates that standardized evaluation of CBF can be performed in large multicenter studies.
Journal of Cerebral Blood Flow & Metabolism (2012) **32,** 1757–1764; doi:10.1038/jcbfm.2012.67; published online 23 May 2012

Keywords: cerebral blood flow; ^{123}I-iodoamphetamine; quantitation; SPECT; vascular reactivity

Introduction

Several imaging modalities for measurement of cerebral circulation have been developed, including positron emission tomography (PET), single photon emission computed tomography (SPECT), perfusion CT, Xe-CT, perfusion magnetic resonance imaging, ultrasonography, and near-infrared spectroscopy. Among these techniques, ^{15}O-PET is excellent in terms of quantitation and space resolution (Frackowiak *et al*, 1980) and can detect the severity of hemodynamic cerebral ischemia as the rise of the oxygen extraction fraction (OEF) (Yamauchi *et al*, 1999). An elevated OEF is defined as misery perfusion (Yamauchi *et al*, 1999), which may be a risk for recurrent stroke and a cause of selective neuronal damage in patients with major cerebral arterial occlusive disease. Therefore, evaluation of the severity of cerebral ischemia is important in predicting prognosis and determining the therapeutic strategy (Yamauchi *et al*, 2007). Ideally, all patients with ischemic cerebrovascular disease should be assessed by PET, but this is impractical because PET facilities are limited. In contrast, SPECT is more commonly available and has broader versatility than PET. Therefore, the use of SPECT for evaluation of the severity of cerebral ischemia could have significant benefits for more patients with ischemic cerebrovascular disorders.

Correspondence: Dr H Yoneda, Department of Neurosurgery and Clinical Neuroscience, Yamaguchi University School of Medicine, 1-1-1 Minami-kogushi, Ube, Yamaguchi 755-8505, Japan.
E-mail: h-yoneda@yamaguchi-u.ac.jp
Received 16 August 2011; revised 3 May 2012; accepted 3 May 2012; published online 23 May 2012

Single photon emission computed tomography cannot be used to observe OEF directly, but quantitation of cerebral blood flow (CBF) using the *N*-isopropy1-[^{123}I]p-iodoamphetamine (IMP) autoradiographic (ARG) method (Hatazawa *et al*, 1997; Iida *et al*, 1994, 1996) can be used to measure thresholds for CBF at rest, determine the cerebrovascular reserve, and detect misery perfusion (Hirano *et al*, 1994). Moreover, the development of the Dual-Table ARG (DTARG) method has made it possible to evaluate CBF at rest and to determine cerebral vascular reactivity (CVR) after acetazolamide challenge using ^{123}I-IMP in a single day session (Kim *et al*, 2006). However, the reproducibility of these methods and standardization among different SPECT models have not been established. In particular, SPECT has a perceived problem that different models of γ-cameras and collimators may give different quantitative values. Therefore, standardization among models and ensuring reproducibility of measured values would be big steps towards utilizing the versatility of SPECT.

To address these issues, QSPECT (quantitative SPECT image reconstruction) has been developed as a program that automatically and accurately corrects attenuated absorption and scattered radiation (Iida *et al*, 1998). This program has been combined with DTARG to give the QSPECT/DTARG method (Iida *et al*, 2010; Kim *et al*, 2006). However, the reproducibility and errors of CBF and CVR measured in the same patients with different SPECT models using QSPECT/DTARG have not been evaluated. In this study, we retrospectively analyzed QSPECT/DTARG data for patients treated at Yamaguchi University Hospital (hereinafter referred to as institution Y) and its affiliated hospital, Ogori Daiichi General Hospital (institution O). These two institutions use different models of γ-cameras and collimators for SPECT, and this provided an opportunity for validation of the reproducibility and determination of the errors of the measured values.

Patients and methods

Patients

The study had a noninterventional, crosssectional design. The protocol was approved by the Yamaguchi University Hospital Institutional Review Board (No. H22-19) and followed the principles of the Declaration of Helsinki. All patient information was anonymized and protected. Among patients who received medical treatment at institution O from September 2005 to August 2009 and were diagnosed with chronic cerebral infarction with cerebrovascular stenosis and underwent QSPECT/DTARG, 25 patients required surgical revascularization and were referred to institution Y, at which QSPECT/DTARG was performed again. Among the 25 patients, 9 (five males and four females) had no differences in medications or clinical conditions at the times QSPECT/DTARG was performed at both facilities. The other 16 patients received additional administration of cilostazol, an antithrombotic agent, before the SPECT examination at institution Y. One of these patients was also treated with pioglitazone for diabetes. Cilostazol and pioglitazone may both increase CBF (Kai *et al*, 2011; Matsumoto *et al*, 2011; Sato *et al*, 2011). Therefore, the 16 patients who received these drugs before the second SPECT examination were excluded because the drugs might have affected the quantitative reproducibility in the study.

Values of CBF in the middle cerebral artery (MCA) territories at rest and after acetazolamide challenge measured at both facilities were examined in these nine patients.

Iodoamphetamine Single Photon Emission Computed Tomography Study Protocol

Procedures for QSPECT/DTARG (Iida *et al*, 2010) are shown in Figure 1. In institution Y, SPECT was performed with a three-headed $\tilde{\alpha}$-camera (GCA-9300A/PI; Toshiba Medical Systems, Tokyo, Japan) and a LESHR fan beam collimator (Toshiba Medical Systems). The energy range was centered at 160 keV with a width of 20%, and 2-minute rotation was performed 14 times in continuous mode. The matrix size was 64×64 pixels. Using the GMS-5500A/PI (Toshiba Medical Systems), fan beam data were converted to parallel data. In institution O, the SPECT machine has a two-headed $\tilde{\alpha}$-camera (E.CAM; Toshiba Medical Systems) and a LMEGP parallel collimator (Toshiba Medical Systems). The energy range was centered on 158 keV with a width of 20%, and 2-minute data collection per 180° was performed 14 times in continuous mode. The matrix size was 64×64 pixels.

In both facilities, an intravenous injection of two bottles of IMP (167 MBq each) was performed at an interval of 30 minutes, using a constant-rate infusion pump (TE-311; Termo, Tokyo, Japan) for 1 minute (Figure 1). Single photon emission computed tomography data collection was started at the same time as the intravenous injection. Dynamic SPECT scanning was performed for 28 minutes with one rotation of 2 minutes performed two times. The first scan lasted from 0 to 28 minutes and the second scan from 30 to 58 minutes, with each scan collecting data for seven frames of four minutes each. At 20 minutes after the first IMP intravenous injection, acetazolamide (Diamox) loading (17 mg/kg) was performed. At 10 minutes after the first IMP intravenous injection, 4 mL of arterial blood was obtained from the radial artery and the standard input function was calibrated. Whole blood radioactivity was measured with a well counter calibrated to the SPECT apparatus. The calibration between the well counter and the SPECT apparatus was performed using a pool phantom with a uniform diameter of 16 cm filled with ~20 MBq of the ^{123}I solution (height; 15 cm), with SPECT scanning using the same protocol as that for clinical testing. The radioactivity of the sampled solution was measured with the well counter used to measure arterial blood radioactivity in clinical testing. For the first and second scans, all frames were summed and images were reconstructed as described below. Gas measurements in the arterial blood were also performed.

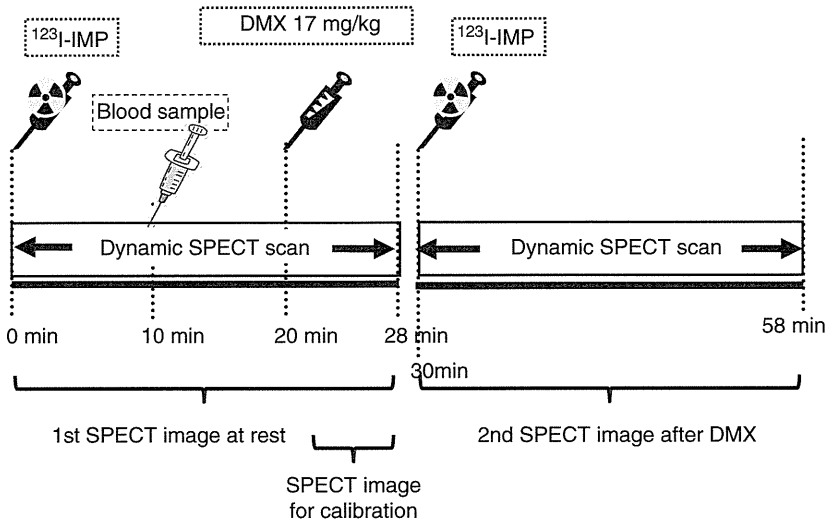

Figure 1 Protocol of the quantitative single photon emission computed tomography/dual-table autoradiographic (QSPECT/DTARG) method. Iodoamphetamine (IMP) was initially intravenously administered for 1 minute and dynamic cerebral blood flow (CBF) SPECT was started simultaneously and continued for 58 minutes (2 minutes × 14 revolutions, two cycles). Ten minutes after IMP administration, arterial blood sampling was performed and an input function was obtained. After 20 minutes, acetazolamide (Diamox) (17 mg/kg) was intravenously administered for 1 minute. After 30 minutes, the same quantity of IMP as in the first administration was intravenously administered for 1 minute. CBF at rest was measured using data collected from 0 to 28 minutes. CBF after acetazolamide challenge was determined using data from 30 to 58 minutes.

Single Photon Emission Computed Tomography Image Reconstruction

Using data from both facilities, images were reconstructed and CBF quantitation was performed using the QSPECT image reconstruction package developed by Iida *et al* (2010) and Kim *et al* (2006). The objectives of QSPECT are to exclude variable factors that occur in SPECT imaging and image reconstruction, to minimize errors between facilities, and to improve quantitation of images. In this software, a series of programs for reconstruction and quantitation are consolidated. Quantitative SPECT extracts head outlines from projection data, makes μ maps, and performs correction of scatted radiation using transmission-dependent convolution subtraction. Transmission-dependent convolution subtraction uses the line spread function obtained from experiments to determine a relational expression among scattered radiation and absorption attenuation coefficient distribution, and the scattered radiation is corrected using this expression. By utilizing the μ map, attenuation correction with ordered subset expectation maximization is performed, the images are reconstructed, and quantitative images are made. These images show the distribution of radioactive concentrations as absolute values expressed as Bq per unit volume.

Single Photon Emission Computed Tomography Image Processing

Single photon emission computed tomography image processing was achieved with the SEE-JET (stereotactic extraction estimation based on the JET study) program (Mizumura *et al*, 2004), using quantitative image data obtained from the QSPECT/DTARG method at rest and after acetazolamide challenge with three-dimensional stereotactic surface projection (3D-SSP). In 3D-SSP, the image tilt of individual subjects is adjusted and linearly converted into 3D stereotaxic coordinates (Talairach standard brain) through the AC–PC line. After anatomic standardization, brain surface extraction is performed with the maximum pixel value shown in the vertical direction in the cerebral cortex from a prescribed brain surface on the stereotaxic coordinate system in the cortex of a standard brain (Minoshima *et al*, 1994). The SEE-JET program can also measure CBF values at rest and after acetazolamide challenge for the territories of the anterior cerebral artery, MCA, and posterior cerebral artery.

The SEE-JET can also automatically calculate the percentage vascular reserve (%VR) for all cerebral coordinate systems, and make 'vascular reserve images'. %VR is defined as ([CBF after acetazolamide challenge−CBF at rest]/CBF at rest) × 100. The program can also classify the severity of hemodynamic brain ischemia for all cerebral coordinate systems into stage 0 to II based on %VR, as described by Nakagawara (1999) and Nakagawara *et al* (2000), and make cerebral surface 'stage images' in 3D-SSP format. The stages are defined as follows: stage 0, resting CBF > 15 mL per minute per 100 g and VR > 30%; stage I, 34 mL per minute per l00 g (80% of normal CBF) > resting CBF > 15 mL per minute per l00 g and 30% > VR > 10%, or CBF > 34 mL per minute per l00 g and 30% > VR > −30%; and stage II, 34 mL per minute per l00 g > resting CBF > 15 mL per minute per l00 g and 10% > VR > −30% (Nakagawara, 1999; Nakagawara *et al*, 2000). Therefore, SEE-JET can perform objective, universal CBF assessment

with automatic analysis that is independent of the operator. The SEE-JET was used on a Windows PC.

Data Analysis

In this study, we investigated CBF in the MCA territories by automatic calculation with SEE-JET. First, Wilcoxon signed-ranks tests were performed on three sets of data for the right and left MCA regions of each patient in institutions O and Y: (1) at rest, (2) after acetazolamide challenge, (3) %VR. Scatter diagrams and linear regression lines were calculated for each data set using Spearman correlation analysis to examine correlations between the two facilities. We also examined interobserver reliability for (1) to (3) using ICCs (intraclass correlation coefficients). Finally, the consistency of MCA CBF measured at the two facilities for each data set was evaluated using Bland–Altman plots (Bland and Altman, 1986). Differences in CBF and %VR were calculated as the value at institution O—that at institution Y. A difference with $P<0.05$ was considered significant.

Results

The subjects were five male and four female patients (59 to 78 years old, mean ± s.d. 68.8 ± 7.1 years old). Five of the patients had ischemic heart disease and one had chronic obstructive pulmonary disease. Four patients were current smokers. Cerebral blood flow in the MCA in each patient in the affected and left hemispheres extracted with SEE-JET, CBF after acetazolamide challenge, and %VR, %Stage II values in the right and left hemispheres are shown in Table 1. These data obtained at the two facilities were compared using Wilcoxon signed-ranks tests. This comparison gave values of $P=0.34$ at rest and $P=0.48$ after acetazolamide challenge for CBF in the right MCA territories ($n=9$); $P=0.91$ at rest and $P=0.64$ after acetazolamide challenge for CBF in the left MCA ($n=9$); $P=0.93$ at rest and $P=0.93$ after acetazolamide challenge for CBF in the right and left MCA ($n=18$); $P=0.24$ for %VR in the right MCA territories ($n=9$) and $P=0.16$ for %VR in the left MCA territories ($n=9$). Therefore, the absolute CBF values and %VR for each patient showed no significant differences between the two facilities.

In Figure 2, three-dimensional cerebral surface CBF extracted images automatically displayed by SEE-JET are shown for data collected in both facilities for patient 3. This patient had symptoms of right internal carotid artery occlusion and the least CVR in the hemisphere among the nine patients. Images from this patient are shown as a representative case. Right and left hemisphere cortical images from both institutions are shown for CBF at rest, CBF after acetazolamide challenge, cerebrovascular reserve, and severity of hemodynamic cerebral ischemia. None of these images showed a major difference between the two facilities, even in a case in which almost all of the right hemisphere was without

?Table 1 Patient characteristics, MCA CBF quantitation, and %stage II values using the SEE-JET program

			Present disease			*Institution O*						*Institution Y*					
						Type of scanner: two-head, parallel-beam collimator						Type of scanner: three-head, fan-beam collimator					
						CBF at rest		CBF after ACZ		%VR[a]		%Stage II[b]	CBF at rest		CBF after ACZ		%VR[a]		%Stage II[b]	
Case	*Age*	*Gender*	IHD	COPD	Smoking	Rt. MCA	Lt. MCA	Rt. MCA	Lt. MCA	Rt. MCA	Lt. MCA	Rt. MCA	Rt. MCA	Lt. MCA	Rt. MCA	Lt. MCA	Rt. MCA	Lt. MCA	Rt. MCA	Lt. MCA
1	74	F	Yes	Yes	—	43.8	42.4	74.7	71.0	70.7	67.2	0.0	0.0	40.2	39.9	63.4	58.6	57.9	47.1	0.0	0.0
2	78	M	Yes	—	Yes	27.6	25.7	45.5	34.3	64.8	33.2	0.0	3.1	29.3	27.7	42.6	35.5	45.6	28.0	0.0	7.1
3	74	F	—	—	—	28.8	35.2	24.8	52.8	−13.9	50.2	83.6	0.0	30.2	33.5	28.4	54.3	−5.9	61.9	69.1	0.0
4	59	F	—	—	Yes	28.9	29.0	49.6	50.5	71.8	74.2	0.0	0.0	31.9	31.6	50.8	50.5	59.3	59.6	0.10	0.0
5	79	M	—	—	—	32.3	35.2	39.7	49.7	22.9	41.1	4.8	0.10	29.3	31.5	31.7	40.5	8.3	28.4	55.1	7.5
6	62	M	Yes	—	Yes	17.7	22.0	20.6	37.6	16.0	71.2	37.6	0.0	24.9	30.7	24.9	42.1	0.08	37.3	71.0	1.7
7	62	F	—	—	Yes	47.7	76.8	64.0	59.7	34.2	−22.3	0.0	0.0	60.0	58.0	65.1	60.9	8.6	5.00	0.0	0.0
8	76	M	Yes	—	—	37.0	31.3	49.6	49.8	34.2	59.3	0.0	0.0	31.5	28.9	33.1	32.0	4.8	10.9	40.2	38.8
9	74	M	Yes	—	—	25.4	23.5	29.8	24.6	17.5	4.7	22.4	67.0	27.7	26.1	32.9	24.0	19.0	−8.2	25.6	69.9

ACZ, acetazolamide; CBF, cerebral blood flow (mL per 100 g per minute); COPD, chronic obstructive pulmonary disease; IHD, ischemic heart disease; MCA, middle cerebral artery; SEE-JET, stereotactic extraction estimation based on the JET study; VR, vascular reserve.

[a]%VR is defined as ([CBF after ACZ−CBF at rest]/CBF at rest) × 100.

[b]Stage II is classified as severe hemodynamic brain ischemia. The %stage II value is the proportion of the Stage II area in the MCA territory.

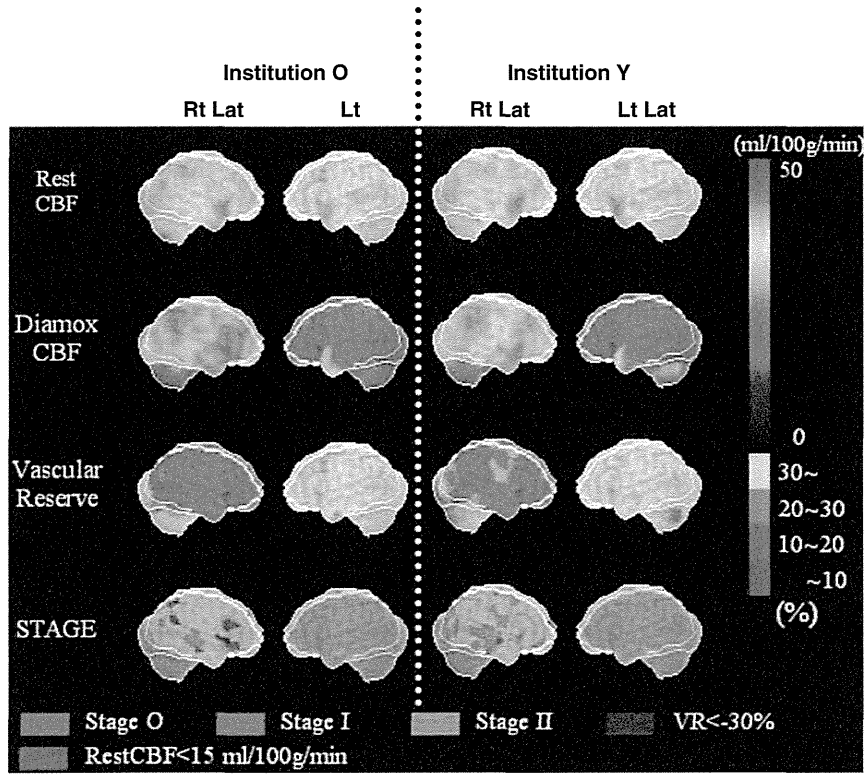

Figure 2 Stereotactic extraction estimation based on the JET study (SEE-JET) images of patient 3 obtained in institutions O and Y. Rt Lat and Lt Lat indicate right hemisphere and left hemisphere outer lateral images, respectively. Cerebral blood flow at rest (Rest CBF), CBF after acetazolamide challenge (Diamox CBF), cerebrovascular reserve (vascular reserve), and severity of hemodynamic cerebral ischemia (STAGE) are shown as three-dimensional cerebral surface images. Images in institutions O and Y are visually almost identical.

cerebrovascular reserve; that is, almost all of the hemisphere had hemodynamic brain ischemia.

In Figure 3, scatter diagrams and linear regression lines comparing data between institutions are shown for MCA CBF in the affected and unaffected hemispheres at rest (Figure 3A), after acetazolamide challenge (Figure 3B), and for %VR (Figure 3C). In Spearman correlation analysis, all four comparisons showed significant correlations between the two facilities (at rest, $r=0.83$, $P<0.01$, $n=18$; after acetazolamide challenge, $r=0.86$, $P<0.01$, $n=18$; %VR, $r=0.82$, $P<0.01$, $n=18$). Regarding interobserver reliability, the ICCs were 0.847 (95% confidence interval (CI): 0.634 to 0.940) for CBF at rest, 0.860 (95% CI: 0.656 to 0.946) after acetazolamide, and 0.727 (95% CI: 0.276 to 0.899) at %VR.

Bland–Altman plots showing the consistency among MCA CBF data measured in the two facilities are shown for MCA CBF at rest (Figure 4A), after acetazolamide challenge (Figure 4B), and for %VR (Figure 4C). For CBF at rest, the mean difference was −0.14 mL per minute per 100 g, the 2 s.d. value was 13.01 mL per minute per 100 g, and 1 of 18 data points was out of the 2 s.d. range. These respective numbers were 3.17 mL per minute per 100 g, 14.39 mL per minute per 100 g, and 1 of 18 data points out of the 2 s.d. range for CBF after acetazolamide challenge; and 12.75%, 34.18% and 2 of 18 data points out of the 2 s.d. range for %VR.

Discussion

Surgical treatment policies for ischemic cerebral diseases have been determined based on the degree of vascular narrowing, as shown in the North American Symptomatic Carotid Endarterectomy Trial study (North American Symptomatic Carotid Endarterectomy Trial Collaborators, 1991). Evaluation of cerebral perfusion has remained at the qualitative level based on relative comparison of the affected and unaffected hemispheres. In recent years, imaging methods such as IMP-ARG (Hatazawa *et al*, 1997; Iida *et al*, 1994, 1996) have been developed and quantitation of CBF has become possible in daily diagnosis. Findings for the relationship between misery perfusion and recurrent symptomatic cerebral infarction suggest that some patients with hemodynamic cerebral ischemia have an increased risk of recurrent ischemic stroke, and that these patients could be detected based on an increase in OEF (Yamauchi *et al*, 1999). Therefore, it is important to evaluate misery perfusion quantitatively to confirm the presence of hemodynamic

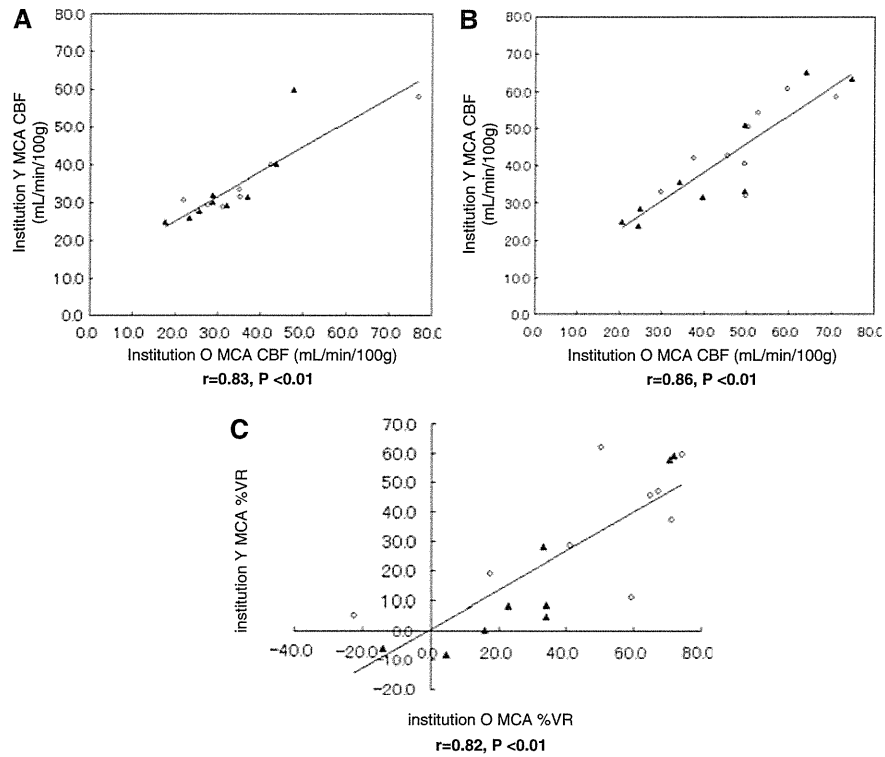

Figure 3 Scatter diagrams and regression lines of middle cerebral artery (MCA) cerebral blood flow (CBF) quantitation and percentage vascular reserve (%VR) in the two facilities. CBF quantitation and %VR in institutions O and Y are plotted on the *x*-axis and *y*-axis, respectively. Data are shown for the affected hemisphere (closed triangles) and the unaffected hemisphere (open circles). There were significant correlations between the two facilities for (**A**) CBF at rest (9 patients, $n = 18$ data points, $r = 0.83$, $P < 0.01$) (**B**) CBF after acetazolamide challenge (9 patients, $n = 18$, $r = 0.86$, $P < 0.01$), and (**C**) %VR for the affected and unaffected hemispheres (9 patients, $n = 18$, $r = 0.82$, $P < 0.01$).

cerebral ischemia, since this may contribute to prevention of recurrent ischemic stroke. To make further progress in this direction, techniques with broad versatility and standardized quantitation are required for large-scale studies.

Positron emission tomography can be used to assess the circulatory and metabolic states in the brain, but only a few facilities have installed PET systems and use of ^{15}O is not common; thus, the versatility of PET is low. In contrast, SPECT is used in most facilities and has broad versatility, but differences in models of γ-cameras and collimators may cause large interinstitutional differences. The QSPECT/DTARG method was developed to resolve errors caused by differences in SPECT models, and we have used this method in our group since December 2004. Such an image reconstruction method with high accuracy and improved quantitation may be helpful for determination of the indication and judgment of the effects of treatment in ischemic cerebral diseases and other diseases. In a multicenter trial, Iida *et al* (2010) found good reproducibility of QSPECT/DTARG. Correction of errors between facilities is also theoretically possible using this method, but this has not been verified by comparison of data from different clinical sites.

In this study, we verified that CBF values measured in nine patients with a cerebral artery stenotic lesion showed reproducibility between facilities. That is, these data showed significant correlations between facilities (institutions Y and O) for CBF at rest ($r = 0.83$, $P < 0.01$), CBF after acetazolamide challenge ($r = 0.86$, $P < 0.01$), CBF at rest and after acetazolamide challenge ($r = 0.91$, $P < 0.01$), and %VR ($r = 0.82$, $P < 0.01$). Good interobserver reliability was obtained, based on respective ICCs of 0.847 (95% CI: 0.634 to 0.940), 0.860 (0.656 to 0.946), 0.872 (0.764 to 0.932), and 0.727 (0.276 to 0.899). A GCA-9300A/PI $\tilde{\alpha}$-camera with three detectors was used in institution Y, whereas an E.CAM $\tilde{\alpha}$-camera with two detectors was used in institution O, and the collimators also differed between the institutions. Despite these differences, strong correlations were found between data collected at the two facilities. This finding is important for performance of multicenter studies. It is also important that the test protocol is strictly defined, as shown in Figure 1, and that the timings of agent administration and blood collection are sufficiently standardized. However, a good correlation was observed in data between the two institutions, both of which followed the test protocol, but there was a tendency for CBF in the higher flow region to

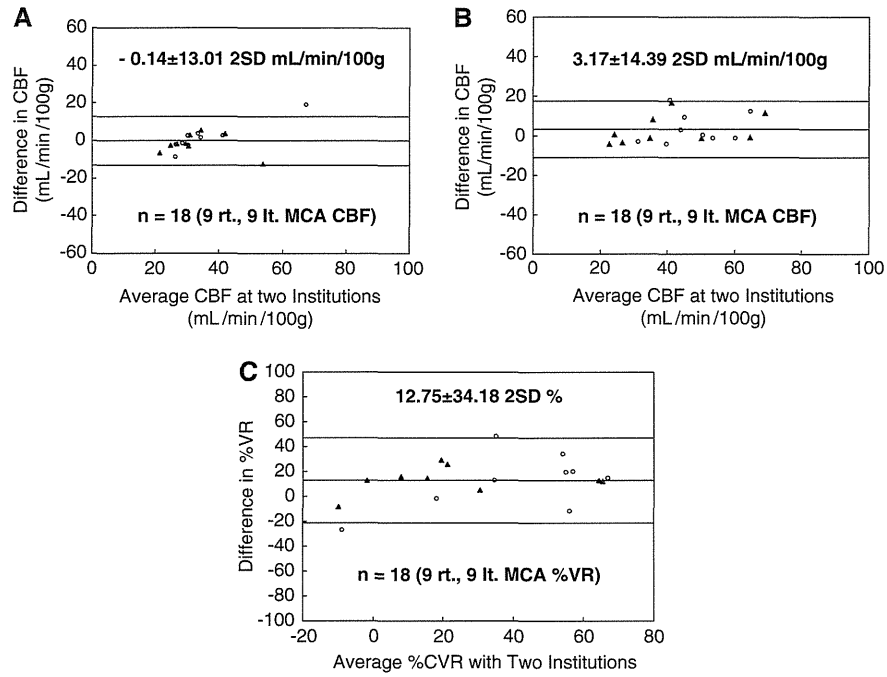

Figure 4 Bland–Altman plots of the consistency of middle cerebral artery (MCA) cerebral blood flow (CBF) measured in the two facilities. Data are shown for the affected hemisphere (closed triangles) and the unaffected hemisphere (open circles). Differences in CBF and percentage vascular reserve (%VR) were calculated as the value at institution O—that at institution Y. (**A**) CBF at rest (9 patients, $n = 18$ data points). A small bias was detected (mean difference, −0.14 mL per 100 g per minute) and the 2 s.d. was moderate (13.01 mL per 100 g per minute). (**B**) CBF after acetazolamide challenge (9 patients, $n = 18$). A small bias was detected (mean difference, 3.17 mL per 100 g per minute) and the 2 s.d. was moderate (14.39 mL per 100 g per minute). (**C**) %VR for the right and left hemispheres (9 patients, $n = 18$). A moderate bias was detected (mean difference, 12.75%) and the 2 s.d. was moderate (34.18%).

be lower at institution Y compared with institution O (Figures 3A and 3B). This might have happened because there was a minimum error when CBF of the same patient was determined with different γ-cameras and collimators using the QSPECT/DTARG method. A further limitation in the study may have been caused by the small sample size. In this study, we focused on data from MCA territories, but the results for the anterior cerebral artery and posterior cerebral artery also showed significant correlations (data not shown).

Good consistency of CBF was also obtained at the two facilities (Figure 4), but some measured values did fall outside the 2 s.d. range. These included one data point for CBF at rest (patient 7, Figure 4A), one after acetazolamide challenge (patient 8, Figure 4B), and two for %VR (patients 7 and 8, Figure 4C). In addition, as seen in Table 1, %VR for the right MCA in cases 7 and 8 at institution Y was significantly lower than that at institution O. In this study, there were no changes in the progress of symptoms and drug administration during the study period for all patients in the two facilities. Furthermore, there were no technical errors in performance of SPECT, time of drug administration, dosage, and leakage in injection. The differences in %VR for patients 7 and 8 suggest a progressive disease phase from the standpoint of cerebral circulation, despite no apparent clinical aggravation. As described above, there were two factors that might have caused the large 2 s.d. range in Figure 4C: the data for Cases 7 and 8 differed significantly between institutions O and Y (Table 1); and the results at institution Y seemed to be slightly lower than those at institution O (Figures 3A to 3C). It was difficult to eliminate intrinsic limitations such as aggravation of cerebral circulation and the reserve of the cerebral circulation because of the retrospective nature of the study. A prospective study with more subjects and a defined observation period is required to confirm the findings of this study.

The QSPECT/DTARG results suggest that this method can be used for objective evaluation as an indication for treatment of ischemic cerebral diseases. In addition, since the reproducibility is high, the method can be applied for observation of time-dependent changes in the same patient. In current medicine, 'standardization' has become important. Standardization of SPECT diagnosis of CBF is important to establish standard therapeutic policies for stroke prevention. This will be facilitated by improved accuracy of quantitative measurements using techniques such as QSPECT/DTARG and of diagnosis of severity using stereotaxic and quantita-

tive image analysis such as SEE analysis. In the current study, CBF assessment with QSPECT/DTARG was significantly correlated between facilities and showed good reproducibility. This method may enable accurate determination of CBF and cerebrovascular reserve capacity at any institution, with standardization of the therapeutic index of patients with ischemic cerebral disease in terms of cerebral circulation.

Disclosure/conflict of interest

The authors declare no conflict of interest.

Acknowledgements

The authors are grateful for excellent technical assistance to Hideyuki Iwanaga and Yona Oishi.

References

Bland JM, Altman DG (1986) Statistical methods for assessing agreement between two methods of clinical measurement. *Lancet* 1:307–10

Frackowiak RS, Lenzi GL, Jones T, Heather JD (1980) Quantitative measurement of regional cerebral blood flow and oxygen metabolism in man using 15O and positron emission tomography: theory, procedure, and normal values. *J Comput Assist Tomogr* 4:727–36

Hatazawa J, Iida H, Shimosegawa E, Sato T, Murakami M, Miura Y (1997) Regional cerebral blood flow measurement with iodine-123-IMP autoradiography: normal values, reproducibility and sensitivity to hypoperfusion. *J Nucl Med* 38:1102–8

Hirano T, Minematsu K, Hasegawa Y, Tanaka Y, Hayashida K, Yamaguchi T (1994) Acetazolamide reactivity on 123I-IMP single photon emission computed tomography in patients with major cerebral artery occlusive disease: correlation with positron emission tomography parameters. *J Cereb Blood Flow Metab* 14:763–70

Iida H, Akutsu T, Endo K, Fukuda H, Inoue T, Ito H, Koga S, Komatani A, Kuwabara Y, Momose T, Nishizawa S, Odano I, Ohkubo M, Sasaki Y, Suzuki H, Tanada S, Toyama H, Yonekura Y, Yoshida T, Uemura K (1996) A multicenter validation of regional cerebral blood flow quantitation using [123I]iodoamphetamine and single photon emission computed tomography. *J Cereb Blood Flow Metab* 16:781–93

Iida H, Itoh H, Nakazawa M, Hatazawa J, Nishimura H, Onishi Y, Uemura K (1994) Quantitative mapping of regional cerebral blood flow using iodine-123-IMP and SPECT. *J Nucl Med* 35:2019–30

Iida H, Nakagawara J, Hayashida K, Fukushima K, Watabe H, Koshino K, Zeniya T, Eberl S (2010) Multicenter evaluation of a standardized protocol for rest and acetazolamide CBF assessment using quantitative SPECT reconstruction program and split-dose 123I-IMP. *J Nucl Med* 51:1624–31

Iida H, Narita Y, Kado H, Kashikura A, Sugawara S, Shoji Y, Kinoshita T, Ogawa T, Eberl S (1998) Effects of scatter and attenuation correction on quantitative assessment of regional cerebral blood flow with SPECT. *J Nucl Med* 39:181–9

Kai Y, Watanabe M, Morioka M, Hirano T, Yano S, Ohmori Y, Kawano T, Hamada J, Kuratsu J (2011) Cilostazol improves symptomatic intracranial artery stenosis – evaluation of cerebral blood flow with single photon emission computed tomography. *Surg Neurol Int* 2:8

Kim KM, Watabe H, Hayashi T, Hayashida K, Katafuchi T, Enomoto N, Ogura T, Shidahara M, Takikawa S, Eberl S, Nakazawa M, Iida H (2006) Quantitative mapping of basal and vasoreactive cerebral blood flow using split-dose 123I-iodoamphetamine and single photon emission computed tomography. *Neuroimage* 33:1126–35

Matsumoto S, Shimodozono M, Miyata R, Kawahira K (2011) Effect of cilostazol administration on cerebral hemodynamics and rehabilitation outcomes in post-stroke patients. *Int J Neurosci* 121:271–8

Minoshima S, Koeppe RA, Frey KA, Kuhl DE (1994) Anatomic standardization: linear scaling and nonlinear warping of functional brain images. *J Nucl Med* 35:1528–37

Mizumura S, Nakagawara J, Takahashi M, Kumita S, Cho K, Nakajo H, Toba M, Kumazaki T (2004) Three-dimensional display in staging hemodynamic brain ischemia for JET study: objective evaluation using SEE analysis and 3D-SSP display. *Ann Nucl Med* 18:13–21

Nakagawara J (1999) Clinical neuroimaging of cerebral ischemia. *No To Shinkei* 51:502–13

Nakagawara J, Hyogo T, Kataoka T, Hayase K, Kasuya J, Kamiyama K (2000) Role of neuroimaging (SPECT/PET, CT/MRI) in thrombolytic therapy. *No To Shinkei* 52:873–82

North American Symptomatic Carotid Endarterectomy Trial Collaborators (1991) Beneficial effect of carotid endarterectomy in symptomatic patients with high-grade carotid stenosis. *N Engl J Med* 325:445–53

Sato T, Hanyu H, Hirao K, Kanetaka H, Sakurai H, Iwamoto T (2011) Efficacy of PPAR-γ agonist pioglitazone in mild Alzheimer disease. *Neurobiol Aging* 32:1626–33

Yamauchi H, Fukuyama H, Nagahama Y, Nabatame H, Ueno M, Nishizawa S, Konishi J, Shio H (1999) Significance of increased oxygen extraction fraction in five-year prognosis of major cerebral arterial occlusive disease. *J Nucl Med* 40:1992–8

Yamauchi H, Kudoh T, Kishibe Y, Iwasaki J, Kagawa S (2007) Selective neuronal damage and chronic hemodynamic cerebral ischemia. *Ann Neurol* 61:454–65

特集 治療可能時間の延長に挑む

ペナンブラを画像化する ②迅速ガスPET検査にむけて

Challenges for Imaging the Ischemic Penumbra
—Towards Ultra Rapid ^{15}O PET System

国立循環器病研究センター研究所画像診断医学部，
同 部長*，国立大学法人香川大学医学部核医学**，
国立循環器病研究センター病院放射線部***，
同 特任部長****

飯田 秀博* *Hidehiro IIDA*
久冨 信行** *Nobuyuki KUDOMI*
三宅 義徳 *Yoshinori MIYAKE*
山田 直明**** *Naoaki YAMADA*
森田奈緒美*** *Naomi MORITA*

KEY WORDS

PET
循環代謝イメージング
急性期脳梗塞
^{15}O 標識酸素
定量化

SUMMARY

^{15}O 標識酸素とPETを使った脳循環代謝量の定量検査法に関して，今までの試みと現状の課題について述べた．検査に要する時間は限りなく短時間化が望ましく，また，多くの作業項目が必要であるため省力化も重要な課題である．筆者らは，専用サイクロトロンと自動合成装置と画像解析ワークステーションの統一管理体系を構築し，限りなく迅速化かつ省力化された検査システムの実用化を目指すものである．

はじめに

^{15}O ガスPET検査は脳虚血性疾患の病態をよく反映し，脳循環代謝諸量の情報量・情報精度において他検査に優ることから，脳血管障害疾患の重症度評価や，適切な治療法の選択において重要な役割を担う．しかしながら，^{15}O は放射線としての寿命が短い（約2分間の半減期）ために院内設置のサイクロトロンが必要である．また，多くのスタッフを必要とし，検査が煩雑であるなどの理由で，多数の症例に用いることは困難であった．また，測定に時間を要し被験者に長時間の安静を強いる制約から，短時間で治療方針決定を求められる急性期医療に応用されることはなかった．本稿では，過去の方法論を振り返り，^{15}O ガスPET検査の意義と技術的課題を明らかにしつつ，脳梗塞医療に貢献するような次世代のPET検査システムについて考察したい．

^{15}O ガス検査の歴史

^{15}O 標識ガスを使ったPET検査は，脳をはじめ全身各組織の酸素代謝量を定量評価できる唯一の手段であるとして，黎明期からその有用性が期待されていた．1970年代後半から1980年代前半にかけて脳血流量や酸素消費量の断層画像が可能になり，理化学研究所の唐沢氏によって開発されたミニサイクロトロンが医療機関での当該検査の発展に重要な貢献を果たした．1980年半ばから1990年前半にかけて秋田脳研の研究チームによって，小型サイクロトロン，^{15}O 標識ガス自動合成装置，定量診断に必要な血中放射能計測装置などの周辺機器，さらに画像計算プログラムが整備され，わが国の^{15}O ガスPET検査の基盤となった．脳梗塞発症後の早期には局所脳血流量が低下するが酸素消費量が維持されて，結果として酸素摂取率が上昇するmisery perfusionの病態，その後酸素消費量が低下するも血流量が上昇するlaxuary perfusionの病態，さらに慢性期におけるmatched perfusionの存在などが明らかになった．脳組織への酸素の運搬機能としての局所脳血流量（組織灌流），および神経細胞の活動を示す直接指標である酸素消費量，これらのバランス指標としての酸素摂取率が，脳虚血性疾患の病態とリスクを適切に表しており，^{15}O ガスPET検査の重要な特長であると考えられ現在に至っている．

^{15}O 標識ガスPET検査では，一連の画像から機能画像に換算するプロセスが必要である．放射性薬剤の数理動態モデルに基づいて行われ，検査プロトコルは理論の前提条件を満たすように組み立てられる．Steady state法では，$C^{15}O_2$ガス吸入（あるいは$H_2{}^{15}O$ 静脈投与）および$^{15}O_2$ガス吸入を定常的に行った後の『平衡時』の画像が，局所脳組織血流量（rCBF），局所酸素代謝量（$rCMRO_2$），および酸素摂取率（rOEF）に依存するとして，単純な計算式にて機能画像を計算する．単一スライスPET装置でも平衡時にベッドを移動することで全脳撮像が可能であるという利点があった．しかし，種々の前提条件を満たすことは困難であり，誤差限界を指摘する報告が多くなされた．放射性ガスを一定の濃度で体内に安定投与すること，および検査中の全身生理機能が常に一定になるようにコントロールすることは現実には容易ではなく，長い検査時間と，吸入マスクの装着による呼吸状態の変化やストレスが血行動態を変化させ，計測の不安定化を来たす（表1）．英国ハマースミス病院で行われた健常者データでは正常者でのrCBF値が90mL/min/100gから30mL/min/100g程度にまで広く分布したが[1]，種々の手技上の誤差だけでなく生理的な変動が反映された結果と考えられた．内部被ばくも大であり，現在の欧州の多くのPET施設では，認めがたいレベルとされる．

その後，各国で体内での放射能濃度分布の平衡を必要としない方法が多く試みられ，1984年にワシントン大学から提案されたボーラス投与autoradiography（ARG法）[2]に改良が加えられ，国内で臨床利用されるようになった．各放射性ガスを吸入直後から短時間PET撮像を行い，一方では，時間とともに変化する動脈血液中の放射能濃度を持続モニターし，これを入力関数とする．脳全体を一度に撮像できるような広い視野を有し，かつ高い感度と計数率特性を保証するPET装置が開発されたことで，この検査が実用的になった．動脈血中の放射能濃度を持続計測する装置[3][4]，血中放射能濃度曲線が脳内放射能濃度と比べて遅延し[5]，かつ変形していること（dispersion）に対する補正法[6]や，^{15}O 酸素吸入検査における動脈血中代謝生成物（^{15}O 水）を補正する方法[7][8]，などが開発され，1時間以内に検査できるようになった．バイパス術やステント留置術，血管内外科術などの血行再建治療の適応決定の指標として有用であるとされ，また，急性期脳梗塞の病態においては，X線CTやMRI撮像法ではよく診断できないような不可逆領域の同定に有用であることが前臨床研究などで明らかになった．1991年には自動合成装置が臨床医療機器としての承認を得たものの，検査は1時間近くに及び，検査は受け入れられ難く，検査中に一定の生理状態を確保することの困難さに加え，サイクロトロンの運転と合成・品質検定作業などにかかる人的配置の困難さから広く利用されるには至っていない．

近年，上記2法よりも検査時間を短縮化させた検査プロトコルが提案された．ひとつはモントリオール大学のSingle Step法と呼ばれる方法であり，1回の$^{15}O_2$ボーラス吸入後の動態からCBF，$CMRO_2$，CBV，OEFの画像をすべて計算するもの

表1 過去の報告における^{15}OガスPET検査のノーマル値

報告者	方法	PET装置	CBF（mL/min/100g）	$CMRO_2$（mL/min/100g）	OEF	CBV（min/100g）	補足事項
Frackowiak RSJ ら（1980）	Steady state 法 閉鎖式フェースマスク	CTI 社 ECAT-Ⅱ	65.3±7.1	5.9±−0.59	0.49±0.2		14名（男11，女3）の健常者，26〜74歳
Lenzi GL ら（1980）	Steady state 法 閉鎖式フェースマスク	CTI 社 ECAT-Ⅱ	64.5±17.3	5.74±1.12	0.49±0.1		27名の健常者，50歳以下と以上を含む
Pantano P ら（1980）	Steady state 法 閉鎖式フェースマスク	CTI 社 ECAT-Ⅱ	52±75	5.0±6.0	0.36±0.5		2名の健常者，57歳，58歳
Yamaguchi T ら（1986）	Steady state 法 開放呼吸式	島津製作所 Headtome-Ⅲ	42.4±7.8	3.28±0.45	0.44±0.06	4.1±0.5	灰白質領域全体，22名の健常者，26〜64歳
Lammertsma AA ら（1990）	持続 $C^{15}O_2$吸入に ARG 法適用 ECAT931-08/12 閉塞式吸入	CTI 社	61±7				同日検査での再現性良好 7名の健常者，33±5歳
Leenders KL ら（1990）	Steady state 法 閉鎖式フェースマスク	CTI 社 ECAT-Ⅱ	54.5±12.3	3.69±0.54	0.39±0.05	5.2±1.4	34名（男16，女18）の健常者，22〜82歳，insular cortex CBF：31.4〜88.8mL/min/100g， $CMRO_2$：2.93〜4.45mL/min/100g， OEF：0.27〜0.50の広い範囲に分布
Hatazawa J ら（1995）	3-step ARG 法 開放呼吸式	島津製作所 Headtome-Ⅳ	61.5±14.7	4.23±0.7	0.42±0.05	4.23±1.04	中側頭回領域，11名の健常者，24〜68歳 Delay 補正が旧法で CBF など20%過大評価
Iida H ら（2000）	3-step ARG 法 開放呼吸式	島津製作所 Headtome-Ⅴ-Dual	39.4±7.3（非採血） 40.5±5.0（動脈採血）				12名（男10，女2）の健常者，22〜69歳
Okazawa H ら（2001）	1-step 3WI 法 開放式で吸入	GE 社 Advance	40.6±4.6	2.19±0.21	0.44±0.04	2.15±0.46	7名（男4，女3）の健常者，37〜55歳，1-step 3WI 法と Steady state 法との比較
	Steady state 法 開放式で吸入		39.8±3.7	2.87±0.17	0.43±0.04	3.7±0.48	
Hattori N ら（2004）	3-step ARG 法 開放式でボーラス吸入	CTI-Siemens 社 ECAT HR+ （3D 収集，Neuroshield 設置）	40.3±5.4	2.85±0.39	0.39±0.06	5.3±1.3	11名（男12，女4）の健常者，35±8歳 （OEF by AV-diff：0.36±0.05）
Ibaraki M ら（2008）	3-step ARG 法 閉塞式フェースマスク	島津製作所 Eminence	53±12	3.5±0.5	0.35±0.06	3.6±0.3	8名の男性健常者，年齢21〜24歳
Bremmer JP ら（1995）	3-step ARG 法 開放式で吸入	CTI-Siemens 社 ECAT HR+	37.3±5.5	3.03±0.2	0.43±0.09	2.98±0.4	別日検査における再現性が良好であることを確認 10名（男6，女4）健常者，平均69（57〜80）歳
Kudomi N ら（2012a）	3-step ARG 法	CTI-Siemens 社 ECAT-47	51.0±3.4	4.27±0.43	0.41±0.03	4.43±0.81	健常者（男性）7名，25.3±2.4歳
	3-step ARG 法の変法 （DARG 法，$H_2{}^{15}O$-$^{15}O_2$-の順） 閉塞式フェースマスク		51.5±3.3	4.28±0.63	0.40±0.04	4.43±0.81	
	3-step ARG 法の変法 （DARG 法，$^{15}O_2$-$H_2{}^{15}O$ の順） フェースマスク使用		50.7±3.8	4.30±0.43	0.41±0.04	4.43±0.81	
Kudomi N ら（2012b）	迅速 DBFM 法 フェースマスク使用	CTI-Siemens 社 ECAT-47	50.8±4.0	4.21±0.65	0.39±0.05	5.89±0.93	健常者（男性）7名，25.3±2.4歳

である（図1）．血液中の代謝生成物（$H_2{}^{15}O$）の影響が考慮されていないことによるバイアスと，画質が不十分だという評価がなされている．もうひとつの方法が国立循環器病研究センターから提案されたDual-Autoradiography（DARG）法と呼ばれる方法で，ARG法における$^{15}O_2$と$C^{15}O_2$あるいは$^{15}O_2$と$H_2{}^{15}O$の投与間隔を短縮させたことで，20分間で検査できる（図1）．$C^{15}O$吸入スキャンを行わずCBV画像の計算も行うことで，さらに検査時間を短縮化するDBFM法も提案されている[9]．^{15}Oガス投与はボーラスかあるいは1分間程度であり，CT搭載型のPET装置を利用すれば全体で検査時間は10分間以内にまで短縮できる可能性がある．全血液中の放射能濃度を持続モニターし，かつ動脈血液中の代謝生成物である$H_2{}^{15}O$を数理モデルで補正する手順はARG法と同様である．

定量精度と信頼性

^{15}OガスPET検査では，局所組織酸素消費量などの生理機能を定量的に計測できるといわれながら，真の意味で正当性の確認がなされているわけではなかった．手技上の誤差は報告ごとに異なるため，CBF，$CMRO_2$の正常値ですら報告によって異なる（表1）．対象群の差やガス吸入法などの違いによる真の差もあるが，撮像パラメータや解析手法の違いも少なからず影響を与える．Itohら[10]は国内の11施設における70名の健常者データにおいての施設間差は，手法や設定したパラメータ数値によるものとしている．

Leendersらの報告においても，健常者のCBFや$CMRO_2$が加齢とともに減少するとしながらも，広い範囲に分散している（CBF値が90mL/min/100gから30mL/min/100g，$CMRO_2$値が2.0mL/min/100gから1.3mL/min/100g）のは，手技上の誤差の影響が大である．閉鎖式のフェースマスクが呼吸を不安定なものにし，2時間を超える検査中の変動が，結果として数値の不安定化を来たしていたと考えられている．^{15}Oガス吸入の安定化を図り，開放マスクの利用をもとに行われたYamaguchiらの報告ではCBFが60mL/min/100g～30mL/min/100g程度，$CMRO_2$が4.3mL/min/100g～2.3mL/min/100gに減少した．表1に示すように，概して開放式の吸入法を採用した報告でCBFが低い傾向を認める．呼吸を安定にさせ，侵襲性を軽減する工夫と検査時間の短縮化が^{15}Oガス検査では本質的であると考えられた．

一般にPETで機能画像の定量化を行うには，数理モデルを仮定して画像計算を行う．$^{15}O_2$吸入ガスPET検査では，脳組織に移行した酸素

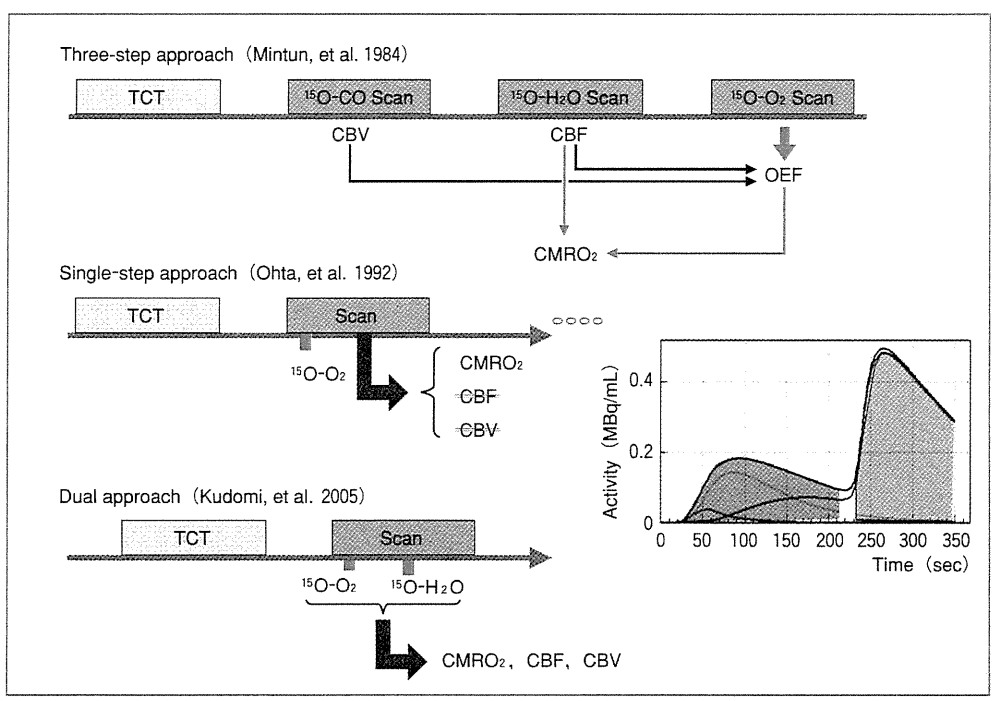

図1 代表的な^{15}OガスPET検査プロトコルの比較

Autoradiographyに代表される3ステップ法では，3つのスキャンごとに異なる放射性薬剤が供給される．1ステップ法では$^{15}O_2$ 1回吸入のみで3つのパラメータを計測することをもくろむが，実際には$CMRO_2$のみが利用される．Dual法では，1回のスキャン中に2種の放射性ガスを吸入する．別に$C^{15}O$吸入スキャンを行うか，あるいは1回のスキャンのみでCBV画像を提示することを試みる．

($^{15}O_2$) は直ちに代謝され $H_2{}^{15}O$ として脳からCBFに従って洗い出される（図2），すなわち酸素としての血液への洗い出しは無視できるほど小さいと仮定している．この仮定は必ずしも実証されたわけではなかったが，近年筆者らの行った検討で，内頸動脈に$^{15}O_2$-標識酸化ヘモグロビンを内頸動脈にボーラス投与した後のクリアランス率が，$H_2{}^{15}O$ をボーラス投与した場合とよく一致することから，本モデルの精度は十分に高いと考える．また，DARG法PET検査をカニクイザル対象に施行したところ，PETで得た脳全体OEF値は内頸静脈の血中酸素分圧から求めたOEF値と，生理的に広い範囲で一致すること（図3）が確認された[11]．迅速化法で初めて示された事実ではあるが，Hattoriらが健常者を対象に確認した報告[12]や，心筋領域におけるOEF定量値の一致に関する報告[13]とあわせて，^{15}O 酸素を用いたPET検査は，きわめて正確に$CMRO_2$やOEF値を計測し得ることを示す．ただし，種々の手技に依存して結果が変わることについても注意が必要で，たとえばHatazawaらの報告[14]では，他報告と比べてCBF値，$CMRO_2$値を約20%高く提示しているが，これは入力関数の遅延（delay）補正における誤差[5]で説明される．このような状況を熟知しておく必要がある．

^{15}O ガスを用いたPET検査で脳循環代謝量を定量評価する場合に，表2に示すような種々の誤差限界がある．PET装置の空間解像度が脳皮質構造と比べると不十分なことに起因する部分容積効果によって，CBFや$CMRO_2$の定量値を過小評価し，その程度はPET装置固有の空間解像度だけではなく，検査プロトコルや解析法によっても異なる．典型的には50%程度の過小評価もあり

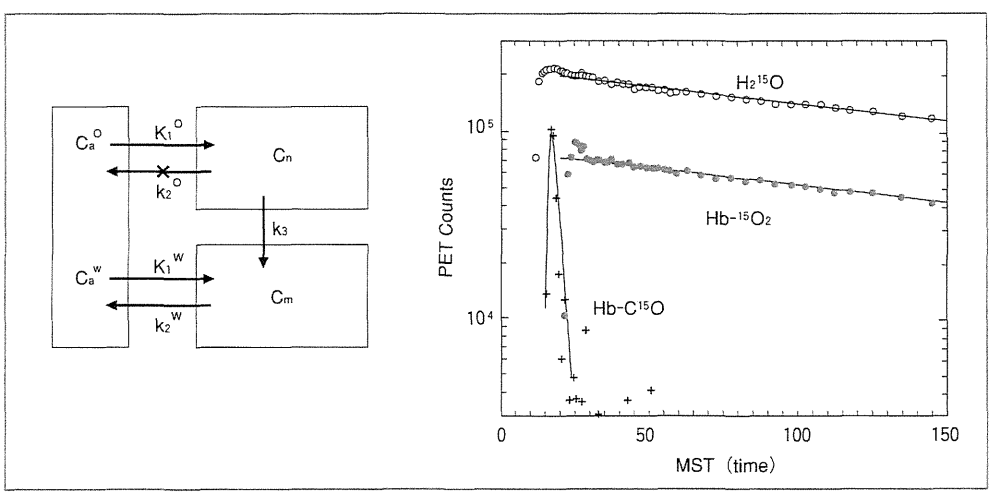

図2 $^{15}O_2$ガスを使った局所脳酸素代謝量（$CMRO_2$）の定量計測の妥当性

脳に移行した$^{15}O_2$は直ちに代謝され$H_2{}^{15}O$としてCBFにて洗い出されると仮定している．実際に内頸動脈に$^{15}O_2$をボーラス投与した後のクリアランスは，同様に$H_2{}^{15}O$を投与した場合のクリアランスによく一致する．脳内に酸素分子として残留する分画がきわめて少ないこと，および酸素代謝量計測に利用される動態モデルの妥当性を示唆している．

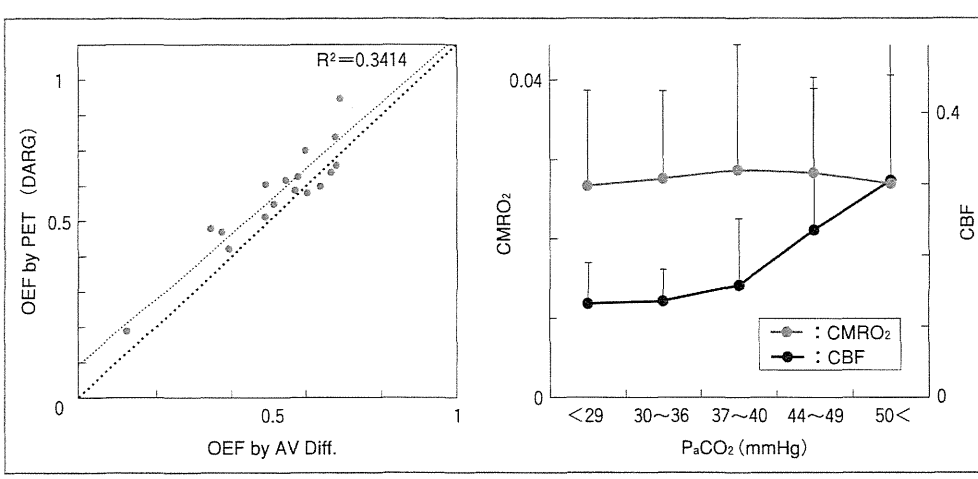

図3 筆者らが行ったカニクイザルを使った妥当性評価の結果

酸素摂取率は内頸静脈採血の酸素分圧から推定した値に，生理的に広い範囲で一致しており，$PaCO_2$に依存していない．^{15}O ガスを使って酸素消費量や酸素摂取率の絶対定量が可能であることを示す．
（文献11より引用改変）

得るとされる[15][16]が，steady state法はARG法やDARG法よりも影響が大きい．ARG法やDARG法では入力関数の遅延（delay）[5]や，これに基づく形の歪み（dispersion）[6]が誤差要因である．動脈採血時におけるdelayを小さくする工夫や，精度の高い補正，誤差を最小化するようなスキャン時間の選択が本質的である．視野内外に強い放射性ガスが存在することや（図4），短い検査での画像精度の確保は必ずしも容易ではなく，投与量や吸入時間，供給マスクやチューブの影響を排除する工夫も必要である．特に高感度化された3次元PET（3D PET）装置ではそれらの影響もより多く受け，本質的な精度限界との競争でもある．しかし，^{15}Oガスを吸入するフェースマスクの改良や投与量の最適化，画像再構成理論の改良などにより，十分に高精度で，高解像度かつ高感度の画像を得ることが可能である（図5，6）．空間解像度や画像精度は従来装置と比べて大きく改善した．PET画像から血中放射能濃度の計測を行うことも可能になり，無採血定量の可能性が広がった．^{15}OガスPET検査の新しい応用領域の開拓に貢献するような今後の研究が期待されるところである．種々の検査手順の簡便化と標準化や，被験者に対する負担の軽減や，生理的変動を最小にする工夫も重要である．

技術的課題

^{15}OガスPET検査を実際の臨床で実施するにはPET撮像と周辺機器の操作だけでなく，動脈採血と血液データの解析，サイクロトロンの運転，一連の^{15}Oガスの標識合成，さらに標識合成ごとにQC（安全性試験，純度検定など）などを担当するスタッフの確保が必要である．検査枠の調整は一般には容易ではなく，急性期脳梗塞疾患の検査への対応は困難であった．筆者らは，オンデマンドでも実施し得る^{15}OガスPET検査システムの実用化を目指して技術整備を行ってきた．^{15}O標識ガス合成装置においては標識合成と品質検定を迅速かつ簡便に実施できるような迅速検査対応型の^{15}Oガス合成システムの開発に成功し，現在4.5分間隔で異なる^{15}O標識ガスを繰り返し供給することが可能になった．すなわち$C^{15}O$ガス吸入を必要とするDARG法検査でも全体で20分間程度，$C^{15}O$ガス吸入を必要としないDBFM法検査では8～9分間程度で一連の検査を完結させることができる．本^{15}Oガス合成・供給装置については，それぞれの放射性ガスを合成，供給終了した後に強制的に排気し，次の標識合成に必要なターゲットガスの充てんを迅速に行う機構を有することが特長であり，

表2 ガスPETの誤差要因

1．部分容積効果
　放射線濃度の系統的誤差
　動態モデルに依存した誤差伝搬
2．入力関数の遅延と歪みに対する補正誤差
　誤差伝搬を抑制するスキャン時間の設定が必要
3．PET装置の誤差，不安定性
　PET装置の誤差，調整不備，etc
　　⇒散乱線補正法の改良
　入力関数モニター装置の誤差（感度の変動，etc）
　Wellカウンター装置の不安定さ（energy windowのズレ，etc）
4．生理的変動に基づく誤差
　真の変動（$PaCO_2$，Hct，Hb，etc）
　変動に伴う計算誤差
5．操作エラーに基づく誤差
　CCF操作，採血操作，撮像のタイミング，etc

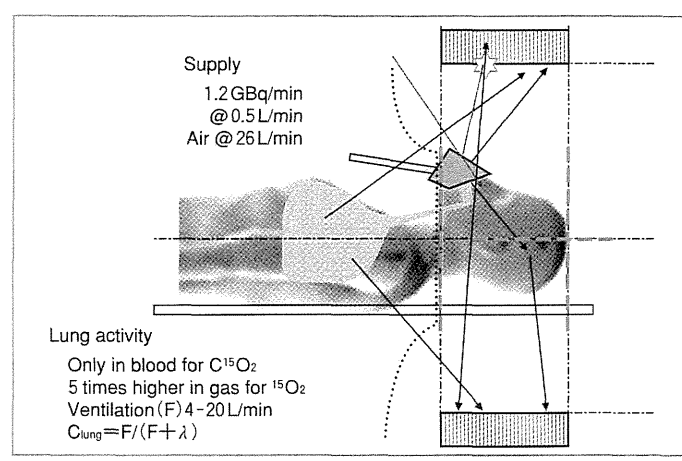

図4 ^{15}OガスPETにおける誤差要因
吸入系における強い^{15}Oガスの影響を排除する工夫が必要である．

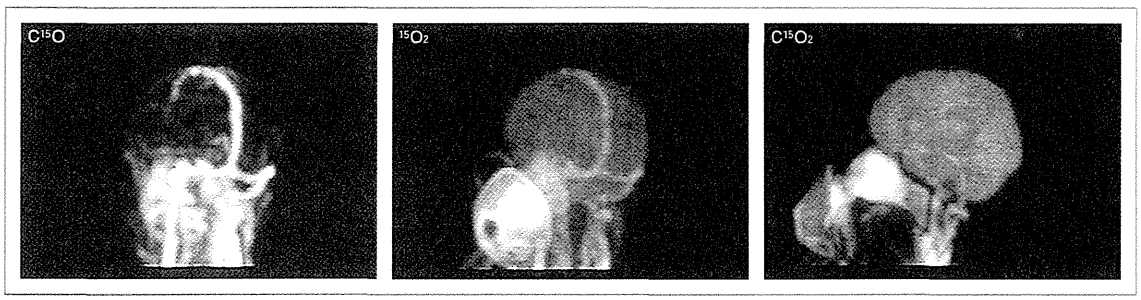

図5 最新の高感度化された3D PET装置で撮像した，$C^{15}O$，$^{15}O_2$，$C^{15}O_2$吸入中の健常者頭部のMIP画像

偶発同時計数，数え落とし，散乱線補正，を正しく補正する物理プロセスを組み込むことで，高感度，高空間解像度，高精度な計測が可能になった．頸動脈などの放射能濃度をモニタするなどの方法を用いることで無採血定量化の可能性が期待される．

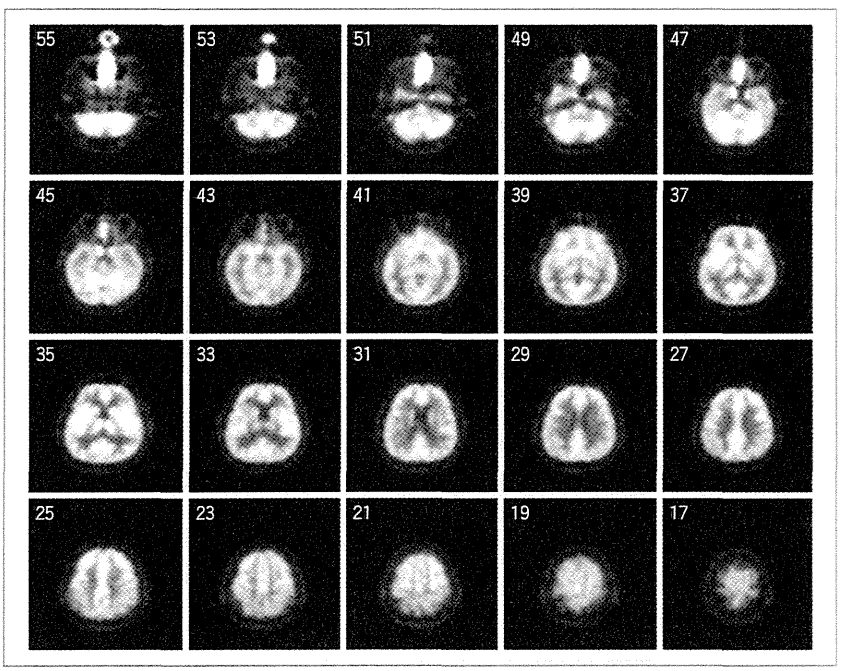

図6 上記3D PETを使って得た健常者の酸素代謝量（定性）画像の例

白質，静脈洞などの分離が鮮明である．

表3 新規^{15}OガスPETシステムにおける改良項目

1．PET画像の精度改善
- 偶発同時係数，数え落とし率の改善
- （3D収集における散乱線補正を含む）
- マスク内放射能の軽減

2．Wellカウンター装置の改良
- Energy windowの確認機能

3．生理的変動に基づく誤差の改善
- マスク内酸素分圧の改善
- 圧迫感の軽減
- 放射性ガスの供給系の安定化
- 検査時間の短縮化

4．手順の軽減
- PETと入力関数の時間調整などの自動化
- 操作の簡便化と作業動線の改善
- 投与量の毎回計測
- 一過性作業の確認機能

医療機器としての装置製造がなされている．さらに^{15}Oガス専用の超小型サイクロトロンと上述の^{15}Oガス合成システムとの組み合わせで，十分な製造能力があることを確認し，それらの一体制御化を試みている．画像解析ワークステーションとの連携，さらに種々の誤差要因を物理的かつソフト的に排除するような工夫（表3）とあわせてシステム構築し，今後有用性と妥当性について検討を行うところである．最終的には，被験者がPET検査室に入室してからの作業動線の効率化，たとえば被験者の固定法やフェースマスクや吸入チューブの装着手順や，$EtCO_2$や血圧，心拍などの生理パラメータのモニタ装置などの接続操作の手順最適化が必要である．このような統合化された検査システムの実用化においては，まさに物理工学研究者と医療スタッフとの共同作業が必要になる．

おわりに

本来，$CMRO_2$は神経細胞のエネルギー代謝を示す指標であり，Mintunら[17]の研究で示されたように，脳組織内の酸素分圧は十分に高いのでCBFは律速段階にはなっていない．一方，CBFは血行力学的な病態だけでなく，種々の神経支配等にも依存して，局所かつグローバルに変化する[18]．このような状況下で脳虚血性疾患におけるOEFやCBF，